

# **A physical based methodology to extrapolate maps of efficiency and corrected mass flow from radial turbines of the type used in turbochargers**

**F. Payri, J.R. Serrano\*, P. Fajardo, R. Gozalbo**

Universidad Politécnica de Valencia. CMT-Motores Térmicos.  
Camino de Vera, s/n. 46022. Valencia, SPAIN.

## **ABSTRACT**

This paper details a physical based methodology to perform an **extrapolation** of the radial turbine performance maps, both mass flow characteristics and the efficiency curve. This method takes into account a narrow range of experimental data, which is usually the data available when such turbines are part of a turbocharger. **Therefore, the extrapolation methodology is especially useful when data from third parties are being used or when the compressor of a turbocharger is used as turbine brake in a gas stand.** The nozzle equation is used to develop an interpolation and extrapolation of the mass flow rate through the turbine. Then, specific information is extracted from this extrapolation and is fed into a total-to-static efficiency equation to carry out an extension of the efficiency curve. This equation is developed using the definition of the total-to-static efficiency, velocity triangles and thermodynamic and fluid fundamental equations.

This procedure has been applied to five radial turbines of different sizes and types. Results are compared against experimental information available in the literature or provided by the turbine manufacturers and a good agreement has been found between theoretical and experimentally estimated data.

**Keywords:** Turbochargers, radial turbines, efficiency and mass flow rate maps extrapolation, physical equations based extrapolation.

\*Contact author:

@mail: [jrserran@mot.upv.es](mailto:jrserran@mot.upv.es)

Phone: + 34 96 387 96 57

Fax: + 34 96 387 76 59

## DEFINITIONS, ACRONYMS, ABBREVIATIONS

<b><math>A_{eff}</math></b>	<i>Equivalent nozzle flow area (<math>m^2</math>)</i>
<b><math>C</math></b>	<i>Absolute velocity (m/s)</i>
<b><math>C_p</math></b>	<i>Gas specific heat at constant pressure (J/kgK)</i>
<b><math>CVT</math></b>	<i>Commercial vaned turbine</i>
<b><math>ER</math></b>	<i>Expansion ratio</i>
<b><math>ER^*</math></b>	<i>Expansion ratio at choked flow conditions</i>
<b><math>h</math></b>	<i>Enthalpy (J/kg)</i>
<b><math>k_i</math></b>	<i>Equation (3) coefficients</i>
<b><math>k', k''</math></b>	<i>Equation (19) coefficients</i>
<b><math>K_i</math></b>	<i>Equations (23,27 and 32) coefficients</i>
<b><math>LSTT</math></b>	<i>Large size truck turbine</i>
<b><math>\dot{m}</math></b>	<i>Mass flow (kg/s)</i>
<b><math>\dot{m}^*</math></b>	<i>Corrected mass flow (<math>kg/s \times T^{0.5}/Pa</math>): <math>\dot{m}(\sqrt{T_{00}}/p_{00})</math></i>
<b><math>MSTT</math></b>	<i>Medium size truck turbine</i>
<b><math>p</math></b>	<i>Pressure (Pa)</i>
<b><math>r</math></b>	<i>Rotor radius (m)</i>
<b><math>R</math></b>	<i>Ideal gas constant (J/kgK)</i>
<b><math>SSTT</math></b>	<i>Small size truck turbine</i>
<b><math>T</math></b>	<i>Temperature (K)</i>
<b><math>U</math></b>	<i>Blade tip velocity (m/s)</i>
<b><math>U^*</math></b>	<i>Corrected blade tip velocity (<math>m/s \times T^{0.5}</math>): <math>U/\sqrt{T_{00}}</math></i>
<b><math>VGT</math></b>	<i>Variable geometry turbine</i>
<b><math>W</math></b>	<i>Relative velocity (m/s)</i>

$\dot{W}$       *Power*

---

### ***Greek symbols***

$\alpha$       *Absolute velocity gas angle*

$\beta$       *Relative velocity gas angle*

$\eta$       *Efficiency*

$\theta$       *Tangential component*

$\rho$       *Gas density (kg/m<sup>3</sup>)*

$\gamma$       *Ratio of specific heats*

$v$       *Blade to jet speed ratio*

$v^*$       *Blade to jet speed ratio at choked flow conditions*

$\Delta$       *Change*

---

### ***Subscripts and superscripts***

$0$       *Stagnation conditions (also indicates inlet turbine conditions)*

$1$       *Conditions at the rotor inlet*

$2$       *Conditions at the rotor exit*

$c$       *Choked flow conditions*

$*$       *Choked flow conditions with ER and  $v$ . Corrected conditions with  $U$  and  $\dot{m}$*

$s$       *Isentropic conditions*

$ts$       *Total-to-static process*

## 1. INTRODUCTION

A way to characterize the performance of a radial inflow turbine widely used in a turbocharger is via a turbine map. Turbine maps usually are presented using two separate plots: one for the mass flow rate and one for the energy conversion efficiency, which usually is taken as the total-to-static efficiency. The former chart is presented as the corrected mass flow ( $\dot{m}^*$ ) as a function of the total-to-static expansion ratio (ER). The corrected mass flow ( $\dot{m}^*$ ) is defined as the mass flow rate multiplied by a ratio between the square root of the turbine stagnation inlet temperature and the turbine stagnation inlet pressure [1]. The other chart is the total-to-static efficiency ( $\eta_{ts}$ ) as a function of the blade to jet speed ratio ( $v$ ), which is a ratio of the rotor tip linear velocity to the isentropic velocity through the turbine stage, for different turbine rotational speeds [1].

Data for constructing this kind of maps is taken from experiments carried out in special test rigs constructed for this purpose. Dale [2] used a test facility built at Imperial College to conduct research on unsteady flow in radial turbines. Winterbone et al. [3] and Nikpour [4] also designed a facility and used a hydraulic dynamometer in order to perform torque measurements. Arcoumanis et al. [5] used a radial compressor instead of a dynamometer to enable increased power of larger turbines to be absorbed. Szymko [6] developed an installation where an eddy current dynamometer was used in order to absorb the power of the turbine and for providing a low known inertia of the rotating assembly, which increases the measurement accuracy of the instantaneous torque.

In the continuous flow test bench at *Universidad Politécnica de Valencia*, the approach is to use a compressor as a braking device [7]. In this last case, a collection of only a narrow range of data is possible, due to the surge and choke limits of the compressor, so a limited widespread of the data is available for constructing the aforementioned turbine maps. Nevertheless, this is a common situation for most of the maps provided by the manufacturers of the turbochargers used in automotive industry. Also, this is standard technique for the OEMs [8][9] of the automotive

industry to characterize turbine maps using the whole turbocharger assembly, due to avoids using special devices of specific knowhow for disassembling, balancing and reassembling the turbine to specific brakes that in the other hand are not commercially available. Nevertheless, new advancements in engine technologies are pushing the limits of operation for turbochargers to low expansion ratios, which in turn brings the analysis of turbine phenomena to higher blade to jet speed ratios [10]. In this region, it is important to have at one's disposal estimations of turbine efficiency; since it gives the possibility to run reliable full engine simulations, this is one of the main reasons stated by Martin et al. [11] to look for techniques to extrapolate turbochargers maps.

This is necessary even when specific turbine models -such as those developed by Benson [12], Payri et al. [13] and Serrano et al. [14]- are used for solving boundary conditions in engine simulation codes, since this kind of models need to be calibrated against a complete enough set of experimental information. Most of the models in the literature are mainly based on empiric or semi-empiric relationships that try to represent different losses that appear along the system, and using them represents the turbine behaviour. An example of this kind of model can be found in [15], included models for the passage losses, tip clearance losses and trailing edge losses. There are several works developing this kind of models for the losses found in the turbine, and specifically the tip losses [16][17]. Other authors [18] have recently developed a 1D model which intends to represent the turbine behaviour under unsteady flow conditions.

It is worth highlighting here that the objective of the methodology purposed in this paper is to extrapolate turbine efficiency and mass flow curves from the range of experimental data usually available, which is generally not wide enough. This objective differences this methodology from the other models that can be found in the literature. The here purposed methodology takes into account these losses (passage, tip, trailing edge, ...) by using the measured data which already include their effects. Having a method which allows estimating the efficiency in regions where there is no experimental data available is a tool which would help in the improvement of engine analysis and

prediction of their operational characteristics. As deduced from the works of Katrasnik [19][20] in advanced engine concepts like hybrids the available 1D models will benefit from more robust physical based methodologies to turbine maps extrapolation. As the methodology proposed for the accomplishment of turbine maps interpolation and extrapolation is based on physical concepts, this will be robust enough to solve the lack of turbine data at off design operative conditions. The aim of this methodology is not to be predictive with a base on geometrical data (only one measured point is not enough); but strictly to extrapolate turbine behaviour from experimental data, one can say that if the range of experimental data available is wide enough, in terms of blade to speed ratio, the methodology here proposed would be closer to a diagnosis model than to a predictive model.

Typical radial turbine maps are shown in figure 1 and figure 2 for the five turbines used in this work. These five turbines are taken as examples for the application of the methodologies and equations presented in this paper. Figure 1 shows three vaneless stator radial turbines' performances maps. For the large size truck turbine (LSTT) information was taken from "Turbo trends and requirements forum" of the 8th International Conference on Turbochargers and Turbocharging [21] (figure 1A) and it was tested in the rig developed by Szymko [6]. The medium (MSTT) and small size (SSTT) turbochargers are also radial, vaneless stator turbines that have been used in a truck engine, as low and high pressure turbines respectively, in a two stage system. The maps for these turbines are shown in figures 1B and 1C and were obtained from the turbochargers manufacturer who tested them in a hydraulic brake test rig for turbine characterization. It can be highlighted that while Figure 1A data was measured at constant turbine corrected speed, Figure 1B and 1C data was measured at constant turbine expansion ratio. Another turbine data that will be used in present work comes from a single stage commercial radial inflow turbine (CVT) used for an analysis carried out by Futral [22] and its main application is the development of power for space applications. Finally, figure 2 shows data from a turbine with nozzles in the stator. The turbine of figure 2 is from a turbocharger of a passenger car engine. It is a small variable geometry turbine (VGT), with

uncambered airfoil section nozzles, which has been tested at *Universidad Politécnica de Valencia* turbochargers test rig [7].

It is worth highlighting that four of the five turbines used to validate proposed extrapolation technique have not been measure at author's laboratory. In spite of this it is possible to know from the literature sources [6][21][22] that all them were tested with air as working fluid and with low turbine inlet temperature. Low turbine inlet temperature means as low as required in order to avoid heat transfer effects, and therefore to be able to measure adiabatic efficiency, but at the same time avoiding freezing air mist at turbine inlet. Futral [18] reports a specific value of 55.74 °C, the VGT was tested in a range between 66°C and 80°C and the rest of the sources does not offer more precision about this datum.

Review literature on test rigs [2] to [7] identifies the different types of gas stands for testing turbochargers in order make clearer the context where the data used in the paper comes from. Nevertheless, the most common source of data are those gas stands that use the compressor of the turbocharger as a break, but they do not produce information in a range of turbine operative conditions wider enough. Therefore, even the proposed methodology is likely to work with data from whatever gas stand it is more useful in the case of those turbine data obtained with the compressor as the turbine break [7].

Detailing paper contents, first a method for the extrapolation of the mass flow chart is proposed based on the nozzle equation (1). The turbine stages are idealized as a single nozzle and a fit of this equation to the mass flow experimental data is carried out to obtain an estimation of the throat equivalent area variation for different blade to jet speed ratio values. In turn, this estimation allows an extrapolation of the mass flow to unknown values of expansion ratio using the same equation. Physical explanation of this behaviour and validation of the procedure for different turbines is provided in section 2. A method for extrapolating the efficiency curve is proposed based on an equation developed from physical principles which involves the definition of total-to-static



efficiency, the velocity triangles for the stage and the thermodynamic behaviour of the flow. It is important for this expression to be a function of the blade jet to speed ratio and some intrinsic data related to any loss mechanisms, geometrical and gas properties, so the turbine can be correctly characterized and the extrapolation can be carried out. The details of the efficiency equation derivation from basic equations are provided in section 3. This equation and the proposed extrapolation procedure are validated with the five different turbines mentioned before: One turbocharger turbine for a passenger car, a set of three turbines composed of a large, a medium and a small size truck turbocharger and a commercial radial inflow turbine for power generation. Details and charts showing validation process results are provided along section 3. Section 4 provides a discussion of the procedure for experimental data extrapolation, where the fitting constants of efficiency equation are analysed and checked against control values. Finally, section 5 is devoted to highlight the main conclusions from the paper.

## **2. EXTENSION OF TURBINES CORRECTED MASS FLOW MAP**

The procedure for the extension of the mass flow map is based mainly on the definition of the subcritical corrected mass flow through the orifice of a single isentropic nozzle. Equation (1), previously introduced, explains the flow behaviour in this situation, a formal demonstration of this expression can be found in the appendix of reference [23]. Some authors have attempted to model the turbine as a single nozzle with some success, for example Watson [1] and Benson [12], and the same basic approach is followed here, but taking into account the possibility for the equivalent nozzle flow area ( $A_{\text{eff}}$ ) -see equation (1)- to be variable instead of a constant value. This fact will be shown later. **Now, considering the corrected mass flow charts described in Figures 1 and 2 and imaging the turbine as a single nozzle, it is possible to say that equation (1) would represent the physical relationship between the corrected mass flow and the expansion ratio if the turbine flow**

behaviour were like a nozzle, which equivalent area is  $A_{eff}$ , and  $A_{eff}$  were not constant but changed for every expansion ratio. That is, providing that gas properties are known (i.e. gamma) and the variation of  $A_{eff}$  is also known for every ER, then it would be possible to plot the entire mass flow curve for any point of operation.

Therefore, the objective will be to estimate  $A_{eff}$  as a function of turbine operative conditions. Equation (1) can also be used to find an indirect operational relationship between  $A_{eff}$  and these conditions; i.e. Total-to-static ER, the corrected speed ( $U^*$ ) or the blade to jet speed ratio ( $v$ ).

$$\dot{m}^* = A_{eff} \sqrt{\frac{\gamma}{R}} \left(\frac{1}{ER}\right)^{\frac{1}{\gamma}} \sqrt{\frac{2}{\gamma-1} \left[1 - \left(\frac{1}{ER}\right)^{\frac{\gamma-1}{\gamma}}\right]} \quad (1)$$

Taking into account the definition of blade to jet speed ratio given in equation (2) and turbine experimental data, which in this case is the corrected mass flow, the expansion ratio and the gas properties; it is possible to calculate the blade to jet speed ratio for every tested point.

$$v = \frac{U}{C_s} = \frac{U^*}{\sqrt{2c_p \left(1 - \left(\frac{1}{ER}\right)^{\frac{\gamma-1}{\gamma}}\right)}} \quad (2)$$

Indeed, for every experimental point of operation there are known values of ER and  $U^*$ . Providing that the basic gas properties (i.e. gamma and  $c_p$ ) are also known, the related blade to jet speed ratio can be obtained via equation (2).

In the case of turbines tested at constant  $U^*$  lines (like the results shown in figure 1A, for the LSTT, and in figure 2, for the CVT and the VGT) it is quite convenient to plot the equivalent area  $A_{eff}$  as a function of the blade to jet speed ratio since a linear trend is obtained. This is shown in figure 3 where  $A_{eff}$  for the LSTT has been plotted, in a dimensionless format, as a ratio with the turbine volute inlet section ( $A_0$ ). The wide operative range of  $v$  that has been able to be measured, thanks to

Szymko device [6], in the case of the LSTT (figure 1A and figure 3) guarantees the consistency of claimed lineal trend. Similar trends were also found by other authors; Zinner [24] and Sanchez et al. [25] proposed direct relationships between  $A_{\text{eff}}$  and ER for a constant turbocharger speed and Muñoz et al. [26] proposed a linear approximation for Zinner relationships. Figure 3 shows some deviations of the linear trend at the smaller speeds and at small values of  $\nu$ , that can be also observed in figure 6.A). The reasons are the higher dispersion in the measurements at lower turbo speeds and principally the intrinsic simplification of the linear trend proposed, which introduce higher errors at the lowest turbo speeds and when the mass flow approaches to choke conditions. As Sanchez et al. [25] deducts, the relation between the area of a nozzle equivalent to the turbine ( $A_{\text{eff}}$ ) and the blade to speed ratio is also affected by the turbine reaction degree and the turbine efficiency and such influence becomes more important as the turbine speed is reduced and ER is increased. Nevertheless, the errors introduced are acceptable to extrapolate corrected mass flow and later on turbine efficiency, as it will be discussed in following section. Figure 4 shows also linear trends for the CVT and the VGT whose maps are shown in figure 2. The narrower operative range tested for the VGT is a drawback as very few points are available for the extrapolation. Nevertheless, the consistent linear trend showed for the wider operative ranges tested with the other two turbines, used to exemplify this phenomenon, allows trusting in the linear trends shown in figure 4B).

On the other hand, when the turbines are characterized at constant expansion ratio, such as the medium and small truck turbines (figure 1B and 1C), this trend changes and becomes quadratic, as it is shown in figure 5. This is not surprising since due to the different testing procedure (at constant ER instead of at constant  $U^*$ ) the operative conditions in the turbine are intrinsically different. Indeed, figure 5 shows that  $A_{\text{eff}}$  decreases at constant expansion ratio (attending to equation (2)  $C_s$  would be constant in these conditions) when turbocharger speed increases. This behaviour is a consequence of the centrifugal force field created by the rotor of the radial turbine [1]. Such a field reduces the mass flow through the turbine for a given expansion ratio (figures 1A and 1B), therefore

the equivalent nozzle that reproduces turbine mass flow behaviour must show a decreasing trend in the  $A_{eff}$  to  $A_0$  ratio. Finally, the decreasing trend shown in figure 5 is quadratic due to the centrifugal forces are proportional to the square of the corrected speed [10].

Nevertheless, it would be expected that independently on which variable has been hold constant during turbine testing ( $U^*$  or ER) the same type of function could relate  $A_{eff}$  to  $A_0$  ratio with turbine operative variables. In addition, from figures 3, 4 and 5 it seems that  $A_{eff}$  to  $A_0$  ratio should be a function of both  $\upsilon$  and  $U^*$ . In this paper the relation shown in equation (3) is proposed:

$$\frac{A_{eff}}{A_0} = k_1 + k_2 \cdot \upsilon \cdot U^* + k_3 \cdot \upsilon + k_4 \cdot U^* \quad (3)$$

Equation (3) has been obtained after exploring several possibilities and considering both the linear trend with  $\upsilon$  and some quadratic behaviour with  $U^*$ . The ' $k_i$ ' coefficients of equation (3) are listed in Table 1 together with the  $R^2$  factor for the three vaneless stator truck turbine maps plotted in figure 1. **Figure 6 shows graphically this relation for these three turbines, where the experimental values are plotted as square points and equation (3) as a surface continue and webbed. In Figure 6, the small segments that join the webbed surface to every square point represent how far the prediction from the experimental value is; the longer is the segment the worst is the prediction.** Since  $R^2$  factor in Table 1 is so close to one, it indicates an average high level of correlation between  $A_{eff}$  to  $A_0$  ratio and the two independent variables ( $\upsilon$  and  $U^*$ ) with the proposed equation (3) structure. Figure 6 shows the constant speed lines in the case of the LSTT and also the previously stated linear behaviour with  $\upsilon$  for this turbine. In addition, in the case of the MSTT and SSTT figure 6 also shows the constant ER lines (from figures 1B and 1C) crossing diagonally the plane  $U^*$ - $\upsilon$ . Since ER is not directly used as an independent variable of equation (3) the quadratic behaviour showed in figure 5 is now represented by the ' $k_2$ ' coefficient in equation (3). Such a quadratic behaviour can be observed appearing in figure 6 as curved surfaces (since equation (3) is

not the equation of a plane surface). Finally, it is worth highlighting that the ' $k_i$ ' coefficients show a trend with turbine size in the case of vaneless stator turbines, specially  $k_1$  and  $k_2$ , as have been represented in the fourth column of Table 1.

Thus, equation (3) in conjunction with equations (1) and (2) are used to fit the experimental mass flow data and to perform an extrapolation of the mass flow map by using the following procedure:

1. Using the data available in the map, equation (1) and equation (2),  $A_{\text{eff}}$  for the experimental points can be calculated and plotted versus the independent variables ( $v$  and  $U^*$ ).
2. Equation (3) is then used to fit the aforementioned calculated  $A_{\text{eff}}$  and values for the ' $k_i$ ' coefficients can be obtained.
3. Evaluating equations (1), (2) and (3) for a wide range of ER and/or  $U^*$ , an extrapolation of the sub critical nozzle equation (1) that fits the experimental mass flow data can be carried out.

Because of the intrinsically sub critical condition of the nozzle equation (1), the mass flow never chokes [23]. Indeed, the curve begins to increase up to a certain  $ER^*$  value and then decreases (figure 7). Obviously, this situation happens when the first derivative of equation (1) is zero. Once this point is reached, the corrected mass flow remains frozen and the corresponding  $ER^*$  can be considered the critical expansion ratio for which choked flow is achieved. Therefore, an extra step can be added to previous procedure:

4. When the first derivative of the sub critical nozzle expression, equation (1), is zero the turbine is choked and, from this point on ( $ER^*$ ), the corresponding value of corrected mass flow is kept constant as the ER is increased.

Results of such extrapolation procedure for the five example turbines are shown in figures 7 to 9.

Figure 7 shows for the LSTT the experimental points and in continuous line the results from the

extrapolation. A dotted line is plotted just to show the non-physical behaviour of equation (1) after critical conditions are reached as well as to identify  $ER^*$  conditions for every  $U^*$ . **It is worth highlighting that the critical conditions of an isentropic nozzle differ from those obtained here ( $ER^*$ ). By two reasons, first because the flow expansion in the turbine is non-isentropic and second because the turbine choking situation is similar to what would happen with two nozzles in series, one equivalent to the stator and another to the rotor[13][14]. In this equivalent case the critical pressure ratio in the whole assembly would be much higher than the critical pressure ratio in only one isentropic nozzle since it is the individual pressure ratio in every nozzle what controls chock flow conditions.**

In figure 8, dotted lines do not appear since  $ER^*$  conditions have not been plotted. Finally, Figure 9 corresponds to the stator vaned turbines, and since measurements were performed at constant  $U^*$  the same graphical code than in figure 7 has been used. It is worth clarifying that some experimental values taken from the CVT analysis (figure 9A) correspond to mass flows values extracted directly from Futral's prediction [22] because of the absence of more experimental information in this reference. In figure 9B the advantages presented by this extrapolation technique can be observed, taking into account the reduced amount of ER values available in the experimental points. The reduced range of ER is due to the fact that the turbine has been tested coupled with the compressor [7], and the compressor is the brake limiting turbine operative range, as it is currently done in any standard gas stand used for turbochargers testing [8].

### **3. EXTENSION OF TURBINES TOTAL-TO-STATIC EFFICIENCY MAP.**

The task of extending the efficiency map must begin with the development of an efficiency equation based on the definition of total-to-static efficiency. **Such definition will be based on equation (4), which may be used only for turbines expanding ideal gas with constant heat capacity.**

Nevertheless, the use of equation (4) is generally accepted [1][8][9] in turbochargers gas turbines if an integral mean value of  $C_p$  and heat capacity ratios is considered to account with turbines gas temperature variation from its inlet to its outlet.

$$\eta_{ts} = \frac{h_{00} - h_{02}}{h_{00} - h_{2s}} = \frac{T_{00} - T_{02}}{T_{00} - T_{2s}} \quad (4)$$

The triangle of velocities for the analysis is presented in figure 10A and the enthalpy – entropy diagram for the turbine stage is also presented in figure 10B. Figure 10B shows stagnation enthalpy and rothalpy points and it is also possible to observe the term corresponding to the rotor centrifugal force field (i.e.:  $(U_1^2 - U_2^2)/2$ ) that is proportional to the square of turbocharger speed, as discussed previously.

Taking into account the velocity triangles, it can be said that:

$$\tan \alpha_1 = \frac{C_{\theta 1}}{C_0} \Rightarrow C_{\theta 1} = C_0 \tan \alpha_1 \quad (5)$$

$$\tan \beta_2 = \frac{x}{C_0} \Rightarrow x = C_0 \tan \beta_2 \quad (6)$$

$$U_2 = x + C_{\theta 2} \Rightarrow C_{\theta 2} = U_2 - x \quad (7)$$

Recalling the general relationship between the lineal velocity and the rotational velocity and applying it to the rotor equation (8) is obtained. In equation (8),  $r_2$  has been defined as the radius that separates in two equal parts the cross section between hub and shroud at turbine wheel outlet.

Figure 10C shows a scheme of turbine wheel diameters and metal angles definitions.

$$\frac{U_1}{r_1} = \frac{U_2}{r_2} \Rightarrow U_2 = U_1 \left( \frac{r_2}{r_1} \right) \quad (8)$$

Combining equations (6) and (8) into (7):

$$C_{\theta 2} = U_1 \left( \frac{r_2}{r_1} \right) - C_0 \tan \beta_2 \quad (9)$$

Recalling equation (4) and assuming ideal gas with constant  $C_p$  it has been obtained equation (10):

$$\eta_{ts} = \frac{h_{00} - h_{02}}{h_{00} - h_{2s}} = \frac{T_{00} - T_{02}}{T_{00} - T_{2s}} = \frac{T_{00} - T_{02}}{T_{00} \left[ 1 - \left( \frac{1}{ER} \right)^{\frac{\gamma-1}{\gamma}} \right]} \quad (10)$$

Combining the definition of turbine power, equation (11), with Euler's equation of turbomachinery, equation (12), whose expression for radial gas turbines can be found in [10] and [25]; it can be obtained equation (13):

$$\dot{W} = \dot{m} \cdot C_p (T_{00} - T_{02}) \quad (11)$$

$$\dot{W} = \dot{m} (U_1 C_{\theta 1} - U_2 C_{\theta 2}) \quad (12)$$

$$T_{00} - T_{02} = \frac{U_1 C_{\theta 1} - U_2 C_{\theta 2}}{C_p} \quad (13)$$

Inserting equation (5), (8), (9) and (13) into (10) and arranging terms:

$$\eta_{ts} = \frac{U_1 C_0 \tan \alpha_1 - U_1 \left( \frac{r_2}{r_1} \right) \left[ U_1 \left( \frac{r_2}{r_1} \right) - C_0 \tan \beta_2 \right]}{C_p \cdot T_{00} \left[ 1 - \left( \frac{1}{ER} \right)^{\frac{\gamma-1}{\gamma}} \right]} \quad (14)$$

Defining  $C_s$  as proposed by Watson [1], i.e.: the velocity which would be attained if the turbine working fluid was expanded in an ideal nozzle over the same expansion ratio as that of the turbine (figure 10), then it can be written:

$$C_s^2 = 2C_p \cdot T_{00} \left[ 1 - \left( \frac{1}{ER} \right)^{\frac{\gamma-1}{\gamma}} \right] \quad (15)$$

Recalling equation (15), then equation (14) can be written as:

$$\eta_{ts} = \frac{-2U_1^2 \left( \frac{r_2}{r_1} \right)^2 + 2U_1 C_0 \left( \tan \alpha_1 + \left( \frac{r_2}{r_1} \right) \tan \beta_2 \right)}{C_s^2} \quad (16)$$

Recalling equation (2) and grouping into  $K_i$  coefficients:



$$\eta_{ts} = -K_1 v^2 + K_2 v \frac{C_0}{C_s} \quad (17)$$

where:

$$K_1 = 2 \left( \frac{r_2}{r_1} \right)^2 \quad K_2 = 2 \left( \tan \alpha_1 + \left( \frac{r_2}{r_1} \right) \tan \beta_2 \right) \quad (18)$$

$K_2$  is further expanded as a function of  $v$  assuming that the angle  $\alpha_1$  (figure 10) has a linear variation with the blade to jet speed ratio, as equation (19) shows where  $k'$  and  $k''$  are constants. This is proposed due to the strong dependence of  $\alpha_1$  flow angle on turbine operative conditions, especially in vaneless turbines [1]. Nevertheless, it is expected a smooth angle variation with  $v$  [22] so the constant  $k'$  should tend to small values near to zero and  $k''$  should tend to values near the geometric value of stator blades angle (in the case of turbines with vaned stator). **These parameters will be addressed latter, in the results discussion section, when the efficiency extrapolation equation will be applied to every studied turbine.**

$$\alpha_1 = k'v + k'' \quad (19)$$

From here on, equation (17) will be used in a different way if the turbine tests have been performed at constant ER or at constant  $U^*$ .

### 3.1. Constant Expansion Ratio Tests

It is necessary to find a relation between  $v$  and term  $C_0/C_s$  in equation (17) in order to make it functional. One way to do that is firstly to replace directly the definitions of the velocities implied in this ratio.  $C_s$  has been already defined in equation (15),  $C_0$  is the circulation velocity (figure 10) and can be found using the continuity equation:

$$C_0 = \frac{\dot{m}RT_0}{p_0A_0} \quad (20)$$

Inserting equations (15) and (20) into  $C_0/C_s$  and solving for the mass flow:

$$\dot{m} = \left( \frac{C_0}{C_s} \right) \frac{p_0A_0}{RT_0} \sqrt{\gamma RT_{00}} \sqrt{\frac{2}{\gamma-1} \left( 1 - \left( \frac{1}{ER} \right)^{\frac{\gamma-1}{\gamma}} \right)} \quad (21)$$

Recalling the equation (1) again, equating with equation (21) and solving for  $C_0/C_s$ :

$$\frac{C_0}{C_s} = \frac{A_{\text{eff}} p_{00} \gamma \left( \frac{1}{ER} \right)^{\frac{1}{\gamma}} RT_0}{p_0 A_0 \gamma RT_{00}} = \frac{A_{\text{eff}}}{A_0} \left( \frac{1}{ER} \right)^{\frac{1}{\gamma}} \left( \frac{T_0}{T_{00}} \right)^{\frac{1}{\gamma}} \quad (22)$$

For hot tests, usually  $T_0/T_{00}$  is close to one (0.997 for this paper temperatures and considering typical  $C_0$  values around 50 m/s), so assuming this simplification and substituting equation (22) into (17), equation (23) is obtained:

$$\eta_{\text{is}} = -K_1 v^2 + K_2 v \frac{A_{\text{eff}}}{A_0} \left( \frac{1}{ER} \right)^{\frac{1}{\gamma}} \quad (23)$$

$A_{\text{eff}}$  to  $A_0$  ratio is further expanded as a function of  $v$  considering that the ratio comes from equation (3).

In equation (23) it is interesting to note that, providing that ER is a constant, the efficiency is zero at a blade to jet speed ratio equal to zero. Assuming a constant value of ER is only possible if the rotor tip velocity ( $U_1$ ) is zero at this condition. This results in a turbine efficiency map crossing through the origin at zero blade to jet speed ratio for every constant ER curve, as it would be expected.

Therefore, equation (23) will be used for extrapolating and analyzing data which has been measured at constant expansion ratio, in this paper this correspond to the data of the SSTT and MSTT. The results obtained from fitting equation (23) to measured data and extrapolating are shown in figure 11.A for the MSTT and figure 11.B for the SSTT. Figure 11 in general shows a good accuracy between measured and calculated efficiency and also shows expected values of  $v$  when extrapolating to zero efficiency values. It is worth noting that the ratio between  $A_{\text{eff}}$  and  $A_0$  has been

obtained using equation (3) and the values used are shown in the corresponding charts from figures 5A and 5B or what are the same figures 6B and 6C.

### 3.2. Constant Corrected Rotor Tip Speed Tests

Nevertheless, it is normal practice (indeed easier if a turbine brake is not available) to measure turbocharger characteristics at constant corrected rotor tip speed rather than at constant ER. Therefore, an expression with this variable as a constant will be necessary. Corrected rotor tip velocity of the turbine is defined as:

$$U_1^* = \frac{U_1}{\sqrt{T_{00}}} \quad (24)$$

Combining equation (24) with (2) and (15) and solving for 1/ER:

$$\left( \frac{1}{ER} \right) = \left[ 1 - \frac{U_1^{*2}}{2C_p v^2} \right]^{\frac{\gamma}{\gamma-1}} \quad (25)$$

Inserting (25) in (22):

$$\frac{C_0}{C_s} = \frac{A_{eff}}{A_0} \left[ 1 - \frac{(\gamma-1)U_1^{*2}}{2\gamma R v^2} \right]^{\frac{1}{\gamma-1}} \left( \frac{T_0}{T_{00}} \right)^{\frac{1}{\gamma}} \quad (26)$$

For turbine operative points located in a constant rotational speed line,  $U_1^*$  is constant and for hot tests usually  $T_0/T_{00}$  is close to one. Therefore, turbine efficiency can be expressed just as a function of  $v$  as equation (27) shows:

$$\eta_{TS} = -K_1 v^2 + K_2^* \left[ 1 - \frac{K_3}{v^2} \right]^{\frac{1}{\gamma-1}} v \quad (27)$$

Where  $K_1$  has been already defined in equation (18) and  $K_2^*$  and  $K_3$  are defined as:

$$K_2^* = 2 \frac{A_{eff}}{A_0} \left( \tan \alpha_1 + \left( \frac{r_2}{r_1} \right) \tan \beta_2 \right) \quad (28)$$

$$K_3 = \frac{(\gamma-1)U_1^{*2}}{2\gamma R} = \frac{U_1^{*2}}{2C_p} \quad (29)$$

$K_2^*$  expression is further expanded as a function of  $\upsilon$  considering that  $A_{\text{eff}}$  to  $A_0$  ratio comes from equation (3) and that the angle  $\alpha_l$  (figure 10) is a linear function of the blade to jet speed ratio, equation (19). Equation (27) has been applied to the turbine data, measured at constant  $U^*$  and described in previous sections, in order to get the efficiency extended map. The results of the extension of these curves are shown (independently for every  $U^*_i$ ) in figure 12 for the LSTT with vaneless stator and in figure 13 for the CVT and VGT with nozzles in the stator. A good accuracy between measured efficiency and the values predicted by equation (27) has been obtained.

In order to get a general view of the entire turbine behaviour, the curves were extrapolated up to efficiency values near zero at both low and high  $\upsilon$  limits. As figure 12 and figure 13 show, zero efficiency (at low  $\upsilon$  values) is obtained at values of  $\upsilon$  higher than zero. This is **due to**  $U^*$  is constant and therefore  $\upsilon$  zero **can only be obtained if  $C_s$  would become infinitum**. The same conclusion can be obtained from the mathematical structure of equation (27), i.e. at  $\upsilon$  zero it is an undetermined equation.

Indeed, figure 12 and figure 13A show the  $\upsilon^*$  values at which choked flow is reached in the turbine [ $\upsilon^*=(U/C_s)^*$ ] for every  $U^*$ , from these points up to lower values of  $\upsilon$  the efficiency should only decrease, as the extrapolation predicts. Nevertheless, such extrapolation at choked flow conditions is not performed using equation (27) as will be discussed in section 3.3.

### 3.3 Choked flow conditions

Since equations (23) and (27) are based in  $A_{\text{eff}}$  to  $A_0$  ratio from equation (3), they are only valid if flow is not choked in the turbine. Therefore, a new expression is needed when dealing with choked corrected mass flow ( $\dot{m}_c^*$ ). Indeed  $C_0$  for choked flow conditions can be written as:

$$C_0 = \frac{\dot{m}RT_0}{P_0A_0} = \frac{\dot{m}_c^*R\sqrt{T_0}}{A_0} \left( \frac{T_0}{T_{00}} \right)^{\frac{2-\gamma}{2\gamma}} \quad (30)$$

Considering equation (27), blade to speed ratio definition (2) and corrected tip speed definition (24) and solving for  $C_0/C_s$  it is possible to obtain such velocity ratio in choked flow conditions, as shows equation (31):

$$\left( \frac{C_0}{C_s} \right)_c = \frac{\upsilon}{U_1} \frac{\dot{m}_c^*R\sqrt{T_0}}{A_0} \left( \frac{T_0}{T_{00}} \right)^{\frac{2-\gamma}{2\gamma}} = \frac{\dot{m}_c^*}{U_1^*} \frac{R\upsilon}{A_0} \left( \frac{T_0}{T_{00}} \right)^{\frac{1}{\gamma}} \quad (31)$$

Therefore, assuming once again that for hot tests usually  $T_0/T_{00}$  is close to one, turbine efficiency for choked conditions can be expressed as:

$$(\eta_{ts})_c = -K_1\upsilon^2 + K_2\upsilon^2 \frac{\dot{m}_c^*}{U_1^*} \frac{R}{A_0} = \upsilon^2 \left( K_2 \frac{\dot{m}_c^*}{U_1^*} \frac{R}{A_0} - K_1 \right) \quad (32)$$

Equation (32) has been used to predict and extrapolate decreasing efficiency at  $\upsilon$  values beyond choked flow conditions in figures 12 and 13. No discontinuity with equation (27) is shown at initial choked flow point; moreover, the results predicted in figure 13.A show good accuracy with experimental data.

#### 4. RESULTS OBTENTION AND DISCUSSION

Since equations (23), (27) and (32) are strongly non-linear with  $\upsilon$ , moreover considering that equations (3) and (19) are embedded inside, the fitting procedure of these turbine efficiency equations to the experimental data must be done using a non linear regression like non-linear least squares computed using for example a Gauss-Newton method with shift-cutting or Levenberg-Marquardt algorithms to avoid divergences. In general those methods are implemented in the most of commercial codes like Statgraphics <sup>(TM)</sup>, SPSS <sup>(TM)</sup>, Matlab <sup>(TM)</sup> or Origin <sup>(TM)</sup>.

The number of parameters that must be fitted is eight, i.e. the four  $k_i$  constants from equation (3), shown in table 1;  $k'$  and  $k''$  constants from equation (19) to determine stator outlet flow angle; and the flow angle at the rotor blade outlet ( $\beta_2$  angle in equation (18) and figure 10). In addition, if there is not available information about turbine geometry and there are enough experimental data measured, as it is the case of the LSTT in present work, another two parameters can be fitted. They are:  $K_1$  coefficient -see equation (18)- related with the ratio of turbine wheel radiuses; and the turbine volute inlet section ( $A_0$ ) that appears in equation (3) and equations (23), (27) and (32). Finally, if there is not information about gas properties either  $K_3$  constant from equation (27) can be also fitted from basic data provided in turbocharger manufacturers maps. In the worst case with a lack of geometry or gas properties information in the map the total number of fitting parameters are eleven.

Usually, when performing this kind of nonlinear statistical fitting, it is necessary to impose initial values to the equation constants and the obtained results are strongly dependent on the provided initial values. For this reason, the initial values for the constants presented in the efficiency equations are collected from experimental information of the turbine geometry. These constants are: The ratio of turbine wheel radiuses for the  $K_1$  coefficient -see equation (18)-, the turbine volute inlet

section for the  $A_0$  constant and the angle at the rotor blade outlet (the metal angle) for the  $\beta_2$  constant (see equation (18) and figure 10).

Figure 14 shows, for the studied turbines, a comparison between the initial values provided to the non-linear fitting procedure (experimentally estimated) and the final values (theoretically calculated) obtained from the procedure as convergence results. These theoretically calculated constants are responsible of the accuracy shown from figure 11 to figure 13 between measured turbine efficiency data and calculated turbine efficiency from equations (23), (27) or (32). Considering the simplicity of the proposed approach and the uncertainty in both turbine efficiency measurements and measurement of geometrical constants, it can be concluded that Figure 14 shows a good agreement between the constants that fit measured efficiency and the experimentally estimated values that has been initially provided. For the LSTT, the experimentally estimated values plotted in figure 14 are just the average of the theoretically calculated ones; this has been done due to the absence of geometrical data in the bibliographical source [21].

Regarding  $K_3$  constant from equation (27) and considering its definition in equation (29), equation (33) is fulfilled:

$$\frac{K_3}{(U_1^*)^2} = \frac{1}{2 \cdot C_p} \quad (33)$$

Therefore, the result of applying equation (33) to the  $K_3$  values (obtained from the non-linear fitting procedure) provides always a value of 0.498 kgK/kJ. As it would be expected, since the turbines tested at constant  $U^*$  that have been described in this paper were tested with air at relatively low temperatures and in these conditions air heat capacity is around 1.004 kJ/kgK.

Finally,  $k'$  and  $k''$  constants from equation (19) provide a certain analysis of  $\alpha_1$  variation with  $\nu$ . Figure 15 shows that there is a small variation of the angle for a wide range of  $\nu$  as it was expected

[22]. Figure 15.A shows the variation of  $\alpha_1$  with the blade to jet speed ratio for the studied turbine with vaned stator. Experimentally estimated values of stator blades  $\alpha_1$  angle (metal angle) are shown in table 2. A reasonable agreement has been obtained between Table 2 data and the corresponding average  $\alpha_1$  values from Figure 15.A.

For the small and medium truck turbines, without stator blades, the  $\alpha_1$  values provided in table 2 has been theoretically estimated assuming momentum conservation in turbine volute and in the vaneless stator [1]. A more significant discrepancy can be observed if the values from table 2 (60° and 62° respectively) are compared to those predicted by the non-linear fitting and shown in figure 15.B. In Figure 15.B the different expansion ratios are shown by the different symbol sizes, the higher is the expansion ratio, the bigger is the symbol. Nevertheless, this result does not diminish the accuracy of the methodology since also according to Watson [1] a high variability of  $\alpha_1$  angle is expected for different operative conditions in vaneless stator turbine. The simple physical equations presented in this paper averaged this variability with a  $\alpha_1$  angle that correctly fits the measured turbine efficiency data. For the LSTT it has not been possible to perform a similar analysis due to the absence of geometrical data in the bibliographical source [21].

Finally, it is worth highlighting that the consistency in the analysis performed of the equations constants (obtained from the non-linear statistical fitting of the results) provides an additional validation of the procedure reliability.

## 5. CONCLUSIONS

A procedure for the extension of both mass flow and efficiency maps for a radial turbine has been shown. It has been illustrated that there is a need for obtaining a good estimation of the efficiency and mass flow in the outer boundaries of the experimental data and a physical based methodology for the accomplishment of this task has been proposed.



Equations for the extrapolation of turbine maps have been developed based on physical principles and a fit procedure to the experimental data has been performed. This methodology of obtaining the extended turbine maps is useful to get a quick estimation of the unknown data and for being implemented into 0D and 1D codes for turbochargers simulation. The obtained results have been compared against experimental information of five different radial turbines obtained from a variety of sources. It has been found a good agreement between physical equations predictions and test data in the two main dependent variables of turbine maps, i.e. turbine isentropic efficiency and turbine mass flow ratio. The good agreement obtained between the measured and the predicted values of these two variables guarantees the quality of the extrapolations obtained with the methodology developed through the paper.

In addition, the extrapolation of measured data performed with the extrapolation has been also validated by an analysis and discussion of the proposed equations constants. This set of equations constants is composed by geometrical data, flow angles and flow heat capacity. These constants have been obtained from a non-linear statistical fitting between proposed equations and experimental data and they shown a consistency with the expected values experimentally and/or theoretically calculated.

## **ACKNOWLEDGMENTS**

The authors wish to thank the economical support for this work to Spanish grant TRA2007-65433/TAIR from Ministerio de Educación y Ciencia. D.G. Investigacion.

## REFERENCES

- [1] Watson, N., Janota, M.S., Turbocharging the Internal Combustion Engine, MacMillan Publishers LTD, London, ISBN 0 333 24290 4, 1982.
- [2] Dale, A.P., “Radial, vaneless, turbocharger turbine performance,” Ph.D. thesis, Imperial College, London, UK, 1990.
- [3] Winterbone, D.E., Nikpour, B., Alexander., G.I., “Measurement of the performance of a radial inflow turbine in conditional steady and unsteady flow,” *IMechE* C405/015. *Proceedings of the 4<sup>th</sup> International Conference on Turbocharging and Turbochargers*, 153 - 162, 1990.
- [4] Nikpour, B., “Measurement of the performance of a radial inflow turbine,” Ph.D. thesis, UMIST, Belfast, UK, 1990.
- [5] Arcoumanis, C., Hakeem, I., Khezzar, L., Martinez-Botas, R.F., Baines, N., “Performance of a mixed flow turbocharger turbine under pulsating flow conditions,” ASME International gas turbine and aeroengine congress and exposition, (95-GT-210), June, 1995.
- [6] Szymko, S., “The development of an eddy current dynamometer for evaluation of steady and pulsating turbocharger turbine performance,” Ph.D. thesis, Imperial College, London, UK, 2006.
- [7] Galindo, J., Serrano, J.R., Guardiola, C. and Cervelló, C., “Surge limit definition in a specific test bench for the characterization of automotive turbochargers,” *Experimental Thermal and Fluid Science* 30, 449–462, 2007.
- [8] CIMAC (The International Council on Combustion Engines), “TURBOCHARGING EFFICIENCIES - DEFINITIONS AND GUIDELINES FOR MEASUREMENT AND CALCULATION” CIMAC Working Group ‘Turbocharger Efficiency’. Number 27/2007.
- [9] SAE J1826, issued 1989-04, Reaffirmed 1995-03, “Turbocharger Stand Test Code”, 1995.
- [10] Moustapha, H., Zelesky, M., Baines, N., Japiske, D. Axial and radial turbines, Concepts

NREC, Vermont, ISBN 0 933283 12 0, 2003.

- [11] Martin, G., Higelin, P., Caillol, C., Talon, V., “Implementing turbomachinery physics into data map-based turbocharger models” SAE Technical Paper 2009-01-0310, 2009.
- [12] Benson, R.S., The thermodynamics and gas dynamics of internal-combustion engines, vol. I, Oxford University Press, Oxford, ISBN 0 19 856210 1, 1982.
- [13] Payri, F., Benajes, J., Reyes, M., “Modelling of supercharger turbines in internal combustion engines,” *Int J Mech Sci.* 8–9:853–69, 1996.
- [14] Serrano, J.R., Arnau, F.J., Dolz, V., Tiseira, A., Cervelló, C., “A model of turbocharger radial turbines appropriate to be used in zero- and one-dimensional gas dynamics codes for internal combustion engines modelling,” *Energy Conversion and Management* 49, 3729–3745, 2008.
- [15] Baines, N. C., “A meanline prediction method for radial turbine efficiency”. 6th International Conference on Turbocharging and Air Management Systems”, *Proc. IMechE*, 3-5 pp 315-325. Paper No. C554-6, November 1998.
- [16] Dambach, R. and Hodson, H.P., “Tip Leakage Flow: A Comparison between Small Axial and Radial Turbines”. *IMechE Sym S. Vol. 767*, 2000
- [17] Dambach, R., Hodson, HP and Huntsman, I. “An experimental study of tip clearance flow in a radial inflow turbine”. *ASME Journal of Turbomachinery. Vol. 121. 4. 644-650.* 1998.
- [18] Macek, J. and Vitek, O. “Simulation of Pulsating Flow Unsteady Operation of a Turbocharger Radial Turbine”. *SAE paper 2008-01-0295*, 2008.
- [19] Katrasnik, T. “Hybridization of powertrain and downsizing of IC engine – A way to reduce fuel consumption and pollutant emissions – Part 1” *Energy Conversion and Management* 48, 1411–1423, 2007.
- [20] Katrasnik, T. “Hybridization of powertrain and downsizing of IC engine – Analysis and parametric study – Part 2” *Energy Conversion and Management* 48, 1424–1434, 2007.

- [21] Martinez-Botas, R. “Opportunities and Challenges. Turbocharger Trends and Requirements Forum”, Annex in the Proceedings of the 8<sup>th</sup> International Conference on Turbochargers and Turbocharging. London, 15-18 May, 2006.
- [22] Futral, S. M., Wasserbauer, C. A., “Off-design performance prediction with experimental verification for a radial-inflow turbine,” NASA Technical Report TN D-2621, 1965.
- [23] Heywood, J., Internal Combustion Engine Fundamentals, McGraw-Hill Science/Engineering/Math, ISBN 0 07 028637 X, 1988.
- [24] Zinner, K., Supercharging of Internal Combustion Engines, Springer-Verlag, New York, ISBN 3 540 08544 0, 1978.
- [25] Sanchez, T., Muñoz, A., Jiménez-Espadafor, F., Turbomáquinas Térmicas. Editorial Síntesis. Chapter 11. Section 7.4. ISBN: 84-9756-185-6, 2004.
- [26] Muñoz, M., Payri, F., Motores de Combustión Interna Alternativos, Sección de Publicaciones de la E.T.S. de Ingenieros Industriales Fundación General – U.P.M, Madrid, ISBN 84-86043-01-9, 1989.

## TABLE CAPTIONS

Table 1:  $k_i$  coefficients for the  $A_{eff}$  to  $A_0$  ratio of the three vaneless stator truck turbines.

Table 2: Estimated values for  $\alpha_1$ . Experimentally from stator blades metal angle for the vaned stator turbines and theoretically for the vaneless turbines

## FIGURE CAPTIONS

Figure 1: Vaneless example turbines (turbine maps). A) LSTT [21]. B) MSTT. C) SSTT.

Figure 2: Vaned example turbine. VGT flow chart and efficiency for certain operative conditions.

Figure 3:  $A_{eff}$  to  $A_0$  ratio versus blade to speed ratio for LSTT. Data measured at constant turbocharger speed [21].

Figure 4:  $A_{eff}$  to  $A_0$  ratio versus blade to speed ratio for the Commercial and the VGT. Column A) CVT [22]. Column B) VGT. Data measured at constant turbocharger speed.

Figure 5:  $A_{eff}$  to  $A_0$  ratio versus blade to speed ratio data measured at constant expansion ratio. A) MSTT. B) SSTT.

Figure 6:  $A_{eff}$  to  $A_0$  ratio versus blade to speed ratio and versus corrected blade speed for stator vaneless turbines. Data measured at constant turbocharger speed (Large [21]) and at constant expansion ratio (Medium and Small)

Figure 7: Corrected mass flow charts versus expansion ratio for the LSTT. Rhombic dots: Measured points [21]. Continuous line: Equation (1) predicted mass flow for subsonic conditions and choked flow for supersonic conditions. Dotted line: Equation (1) predicted mass flow for subsonic flow conditions.

Figure 8: Corrected mass flow charts versus turbocharger speed. A) MSTT. B) SSTT

Figure 9: Corrected mass flow charts versus expansion ratio for vaned stator turbines. Column A) CVT [22]. Column B) VGT. Rhombic dots: Measured points. Continuous line: Equation (1) predicted mass flow for subsonic conditions and choked flow for supersonic conditions. Dotted line: Equation (1) predicted mass flow for subsonic flow conditions.

Figure 10. A) Velocity triangles for constant meridional component velocity in a radial turbine. B) Enthalpy versus entropy diagram for the turbine stage. C) Definition of dimensions and metal angles in the turbine rotor.

Figure 11: Isentropic efficiency fit for vaneless stator turbines; data measured at constant expansion ratio. A) MSTT. B) SSTT. Rombic dots: Experimental data. Continuous line: Equation (23) predicted efficiency.

Figure 12: Isentropic efficiency fit for the vaneless stator LSTT. Experimental data measured at constant corrected speed [21]. Rhombic dots: Experimental data. Continuous line: Equation (27) predicted efficiency.

Figure 13: Isentropic efficiency fit for vaned stator turbines; data measured at constant turbocharger speed. A) CVT [22]. B) VGT. Rhombic dots: Experimental data. Continuous line: Equation (23) predicted efficiency.

Figure 14:  $K_1$  coefficient,  $\beta_2$  angle and  $A_0$  for five turbines from the studied set.

Figure 15: Variation of  $\alpha_1$  versus blade to speed ratio. A) Example turbines with vaned stator. B) Example turbines with vaneless stator. In B) chart size reduction in triangles and circles indicates expansion ratio reduction for a given turbine.

TABLES

Table 1:  $k_i$  coefficients for the  $A_{eff}$  to  $A_0$  ratio of the three vaneless stator truck turbines

Coefficient	Large size	Medium size	Small size	$k_i$ coefficient trend with turbine size
$k_1$	0.50	0.32	0.20	↓
$k_2$	-0.30	-0.25	-0.13	↑
$k_3$	-0.20	-0.13	-0.19	≅
$k_4$	0.35	0.34	0.31	≅
$R^2$	97	97	99	

Table 2: Estimated values for  $\alpha_1$ . Experimentally from stator blades metal angle for the vaned stator turbines and theoretically for the vaneless turbines

Turbine type	$\alpha_1$
Vaned Stator CVT	63°
VGT Passenger car 0% opening	83°
VGT Passenger car 50% opening	64°
VGT Passenger car 100% opening	43°
SSTT (vaneless)	60°
MSTT (vaneless)	62°

FIGURES

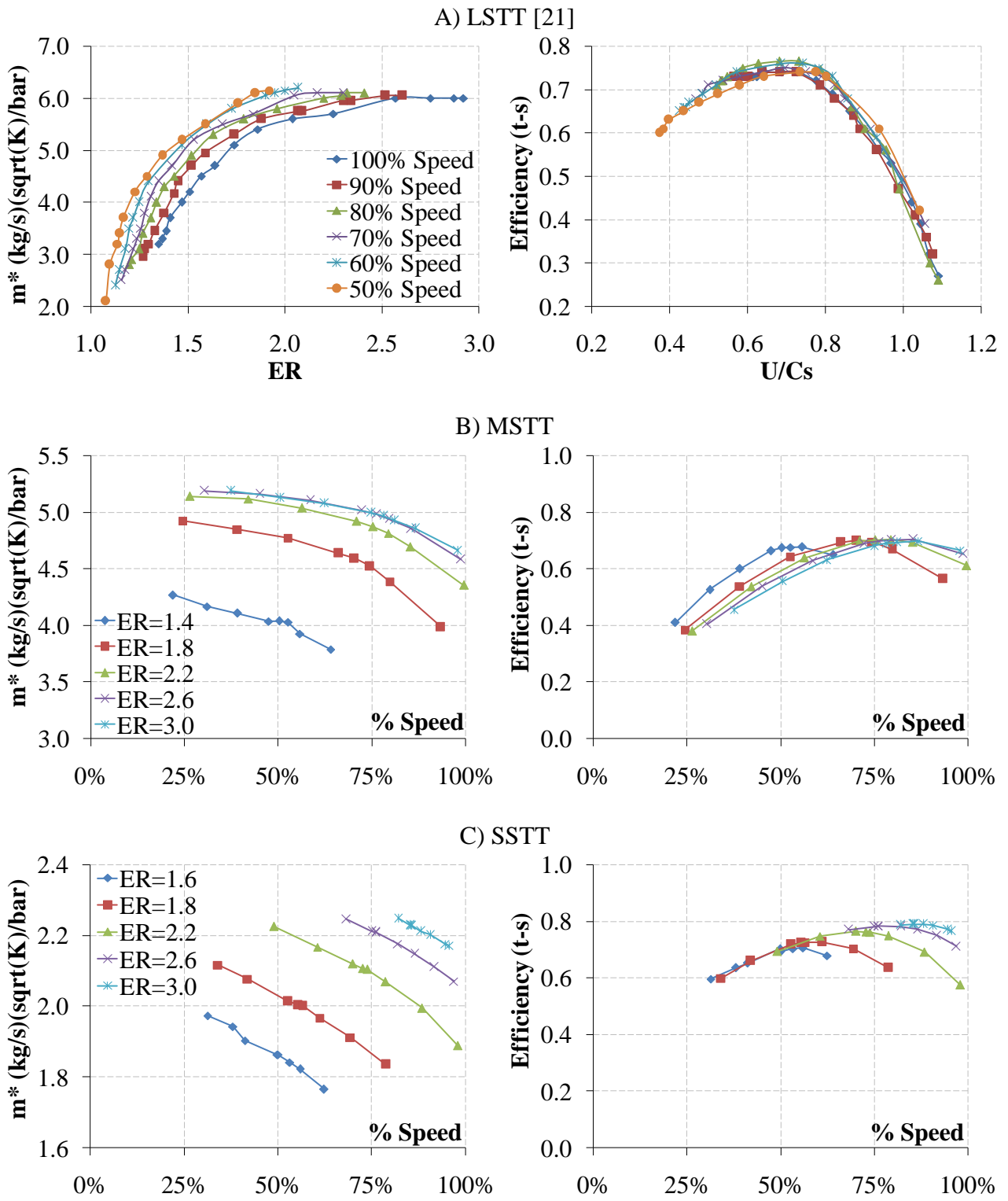


Figure 1: Vaneless example turbines (turbine maps). A) LSTT [21]. B) MSTT. C) SSTT.



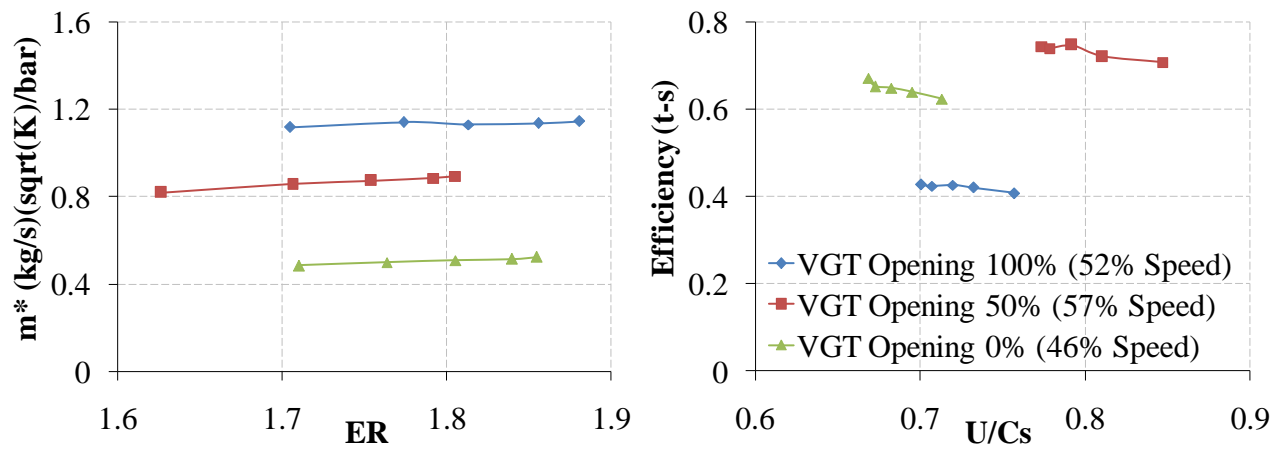


Figure 2: Vaned example turbine. VGT flow chart and efficiency for certain operative conditions.

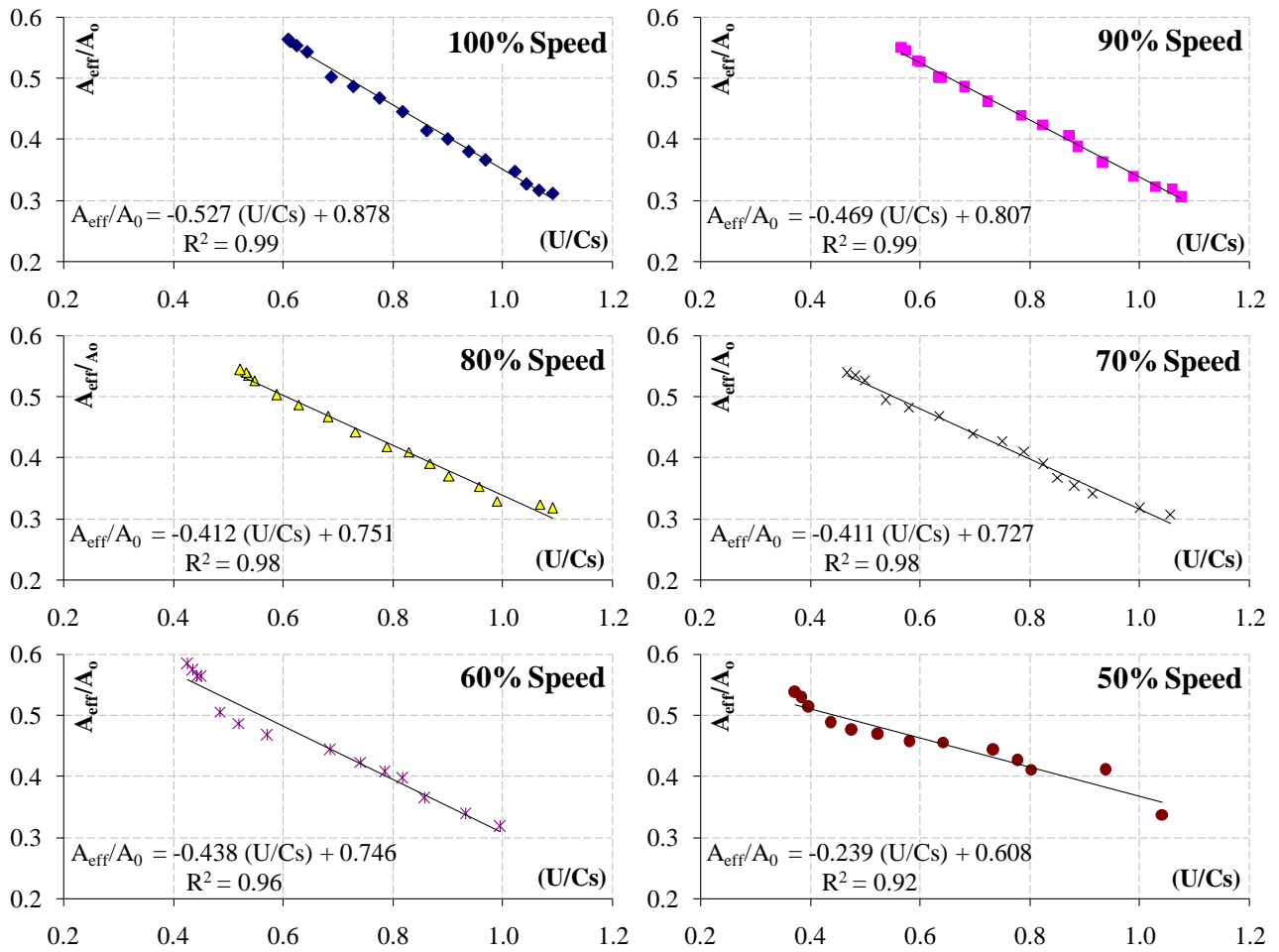


Figure 3:  $A_{eff}$  to  $A_0$  ratio versus blade to speed ratio for LSTT. Data measured at constant turbocharger speed [21].

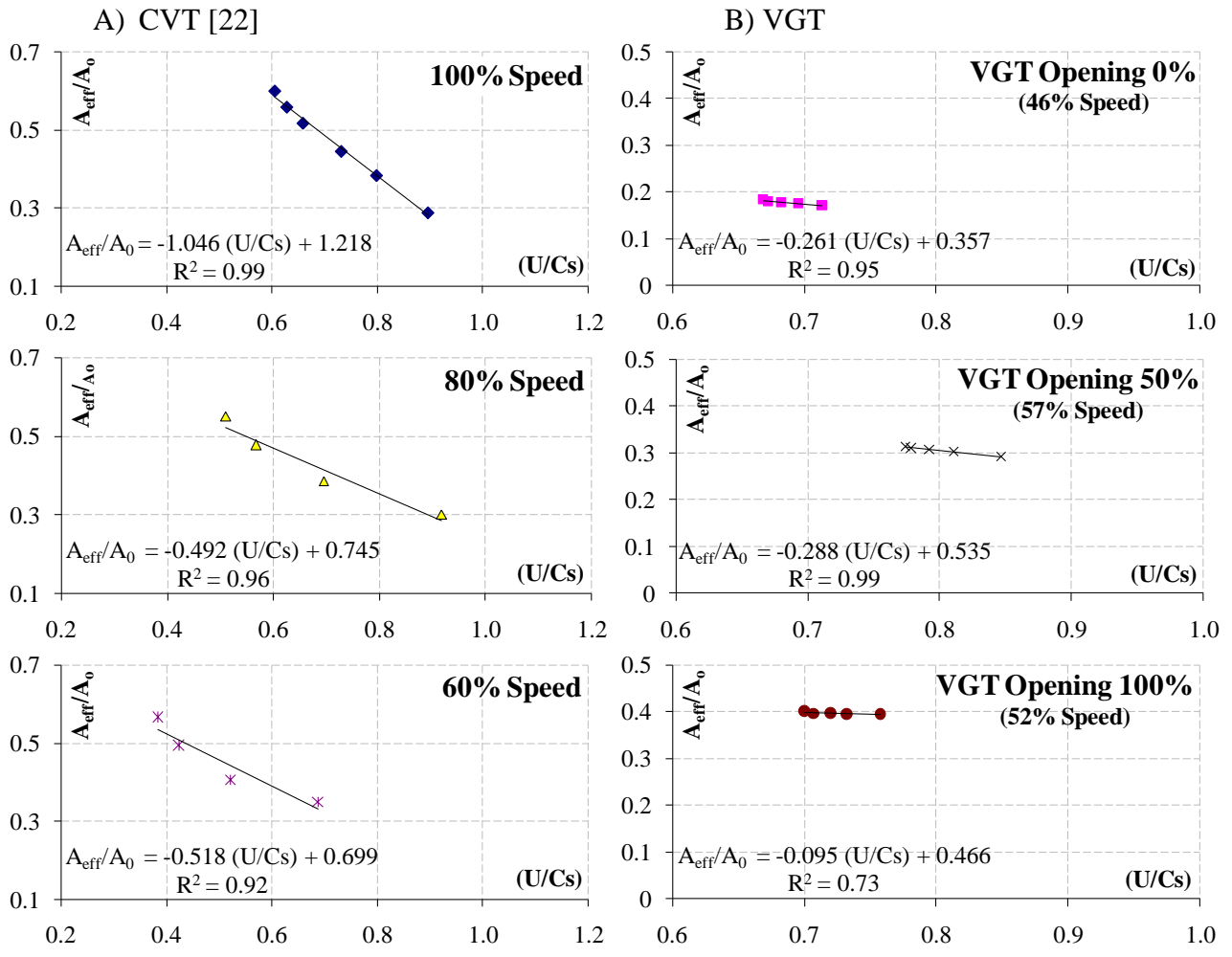


Figure 4:  $A_{eff}$  to  $A_0$  ratio versus blade to speed ratio for the Commercial and the VGT. Column A) CVT [22]. Column B) VGT. Data measured at constant turbocharger speed.

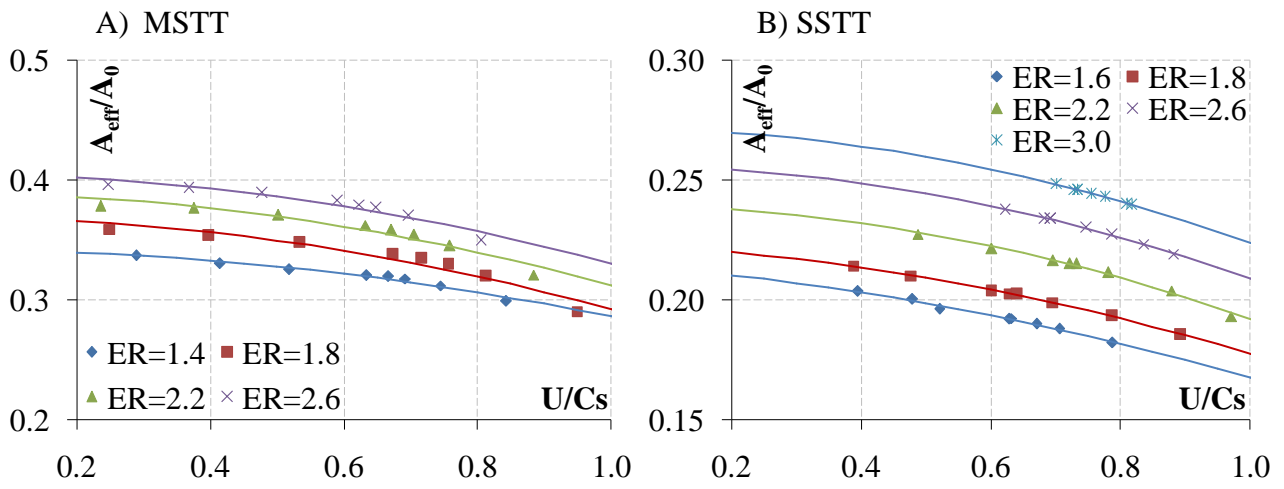


Figure 5:  $A_{eff}$  to  $A_0$  ratio versus blade to speed ratio data measured at constant expansion ratio. A) MSTT. B) SSTT

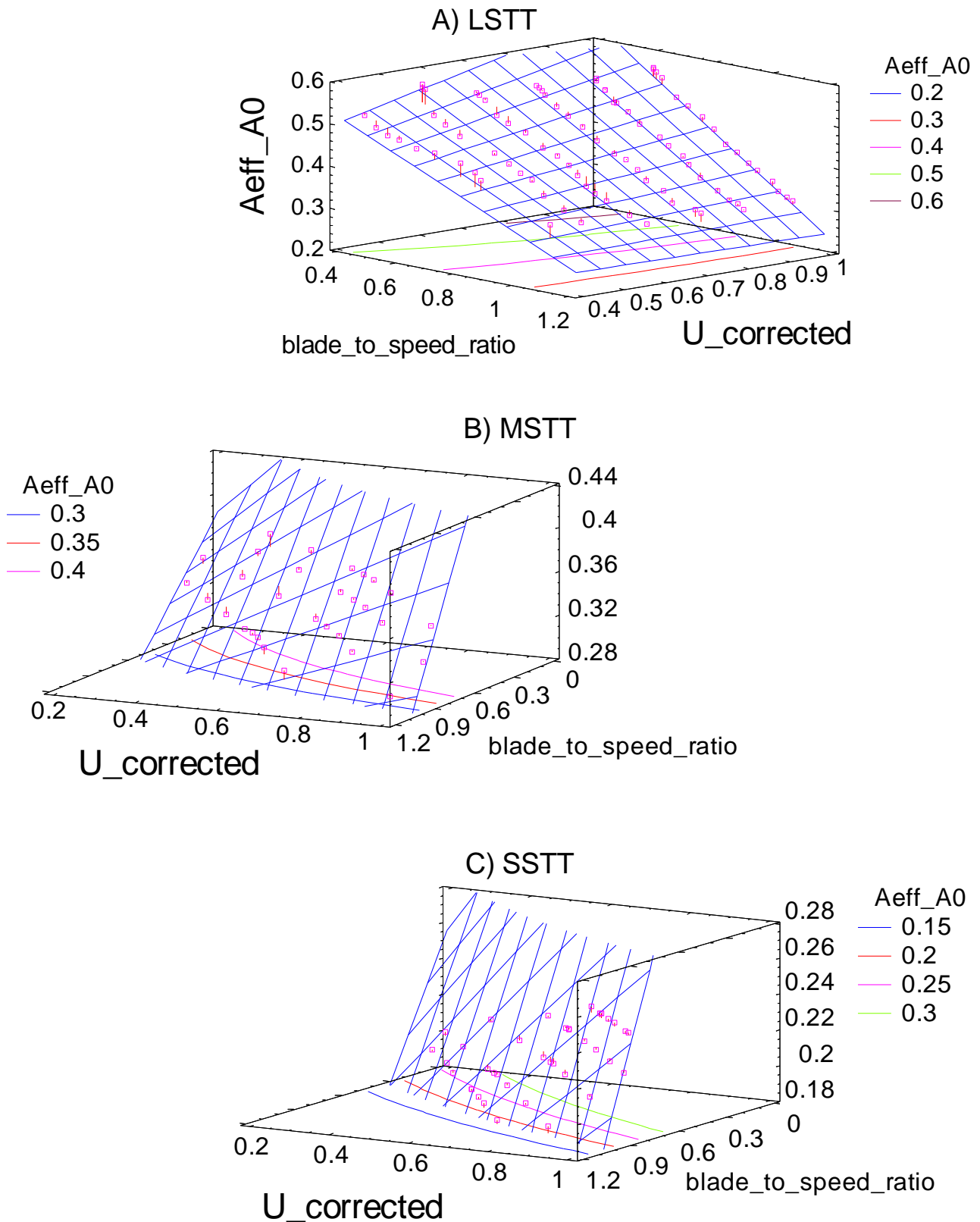


Figure 6:  $A_{eff}$  to  $A_0$  ratio versus blade to speed ratio and versus corrected blade speed for stator vaneless turbines. A) Data measured at constant turbocharger speed (LSTT [21]) B) and C) Data measured at constant expansion ratio (MSTT and SSTT)

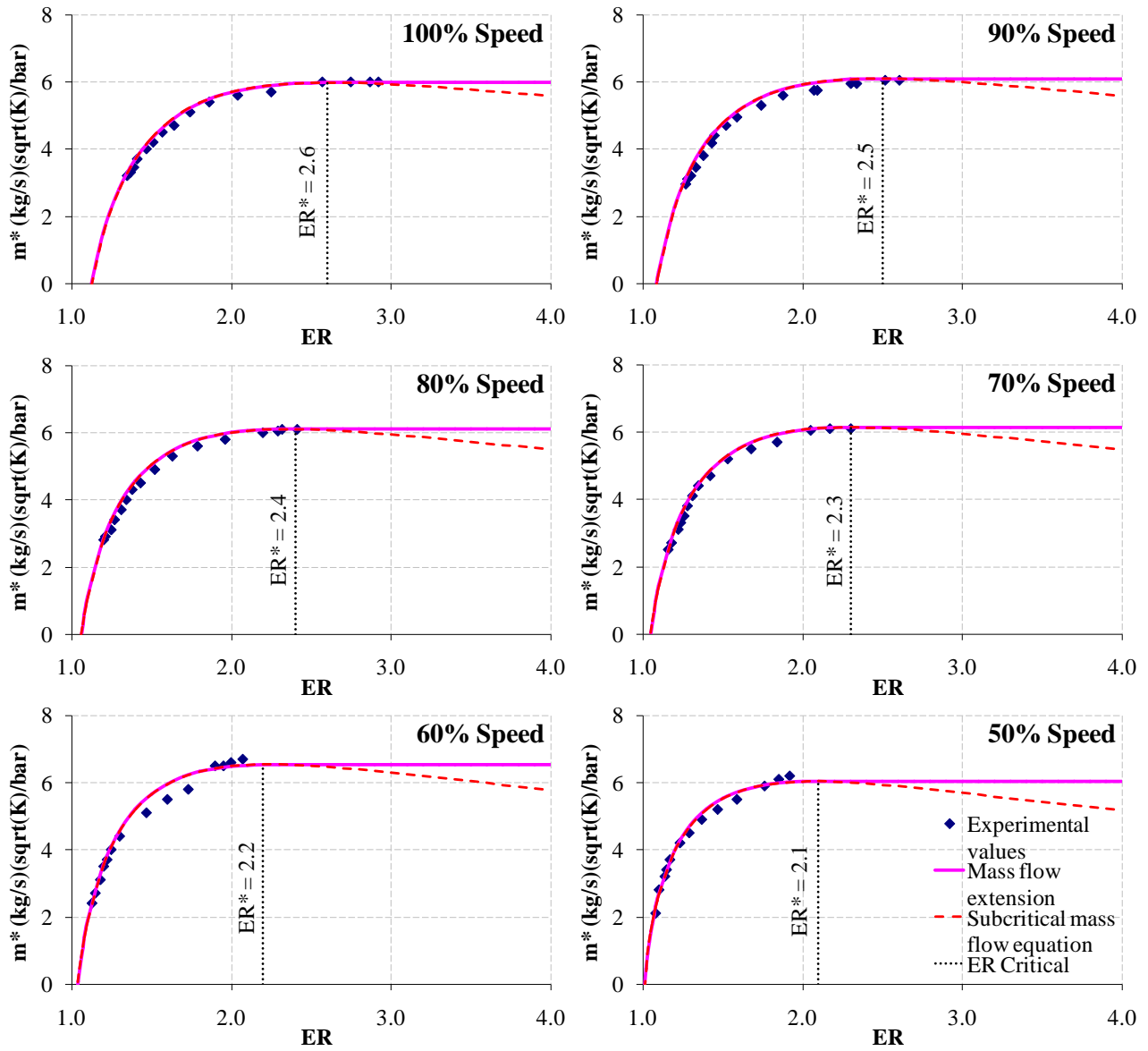


Figure 7: Corrected mass flow charts versus expansion ratio for the LSTT. Rhombic dots: Measured points [21]. Continuous line: Equation (1) predicted mass flow for subsonic conditions and choked flow for supersonic conditions. Dotted line: Equation (1) predicted mass flow for subsonic flow conditions.

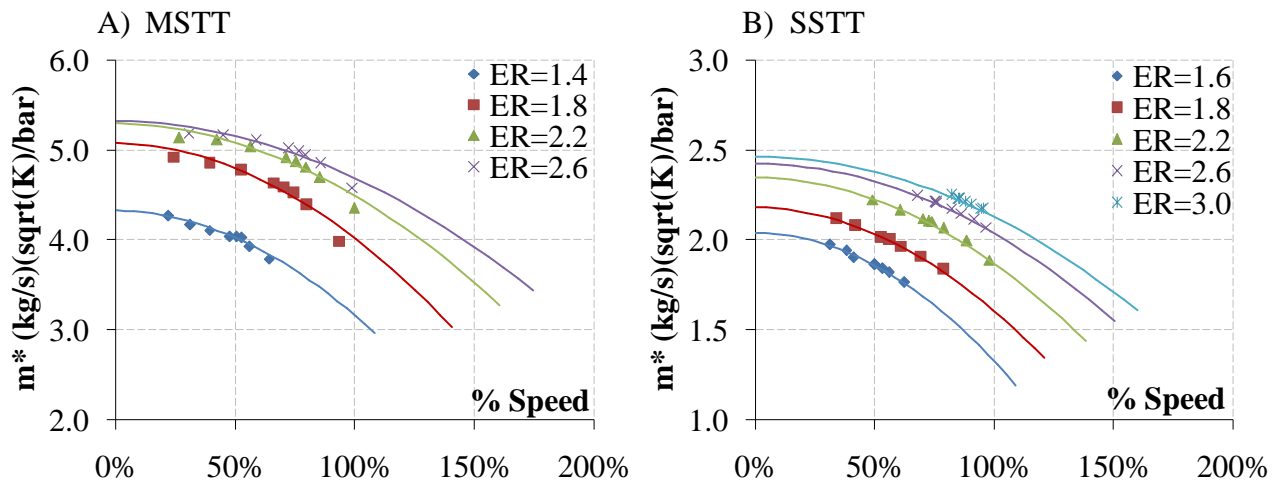


Figure 8: Corrected mass flow charts versus turbocharger speed. A) MSTT. B) SSTT

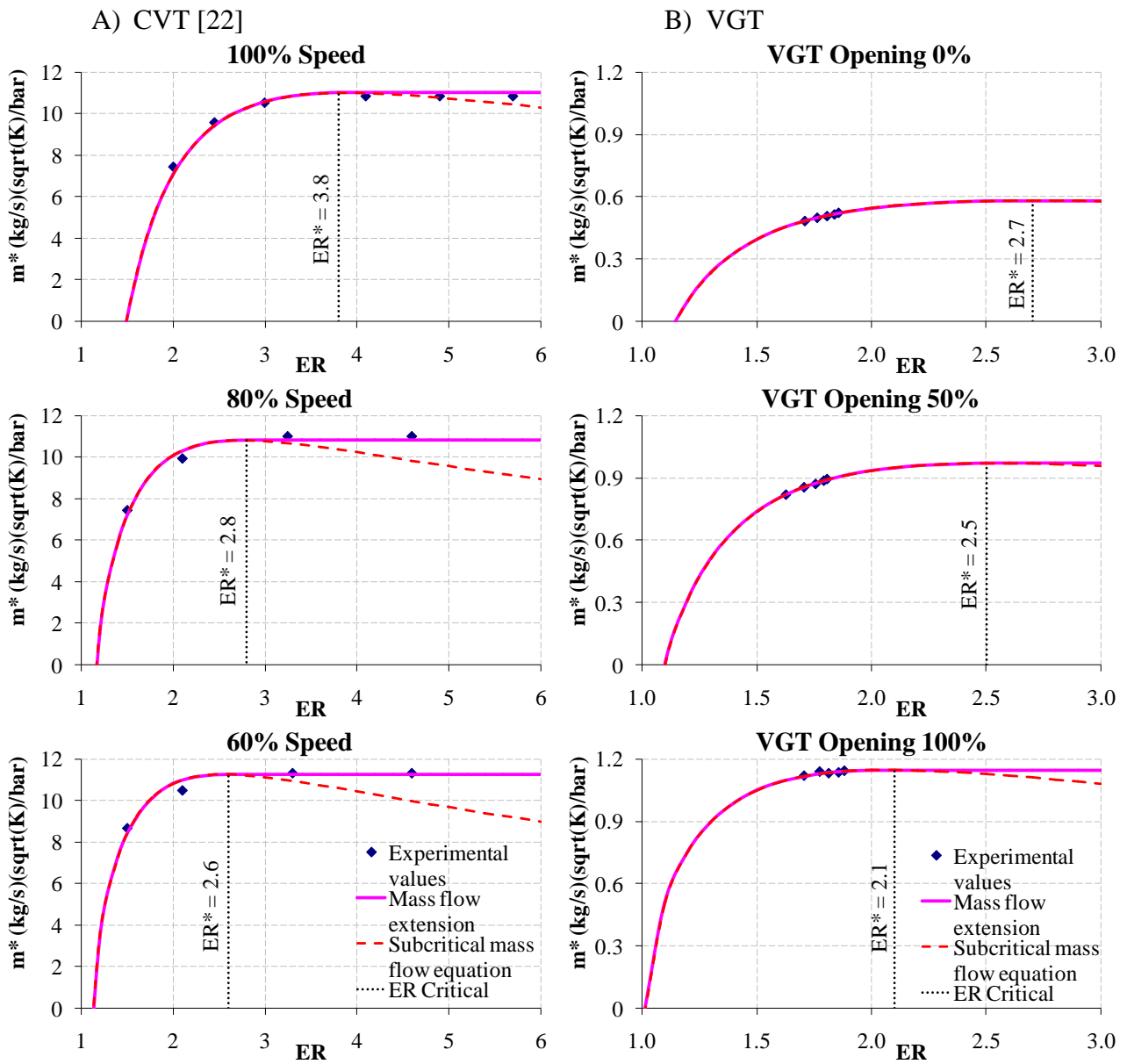


Figure 9: Corrected mass flow charts versus expansion ratio for vaned stator turbines. Column A) CVT [22]. Column B) VGT. Rhombus: Measured points. Continuous line: Equation (1) predicted mass flow for subsonic conditions and choked flow for supersonic conditions. Dotted line: Equation (1) predicted mass flow for subsonic flow conditions.



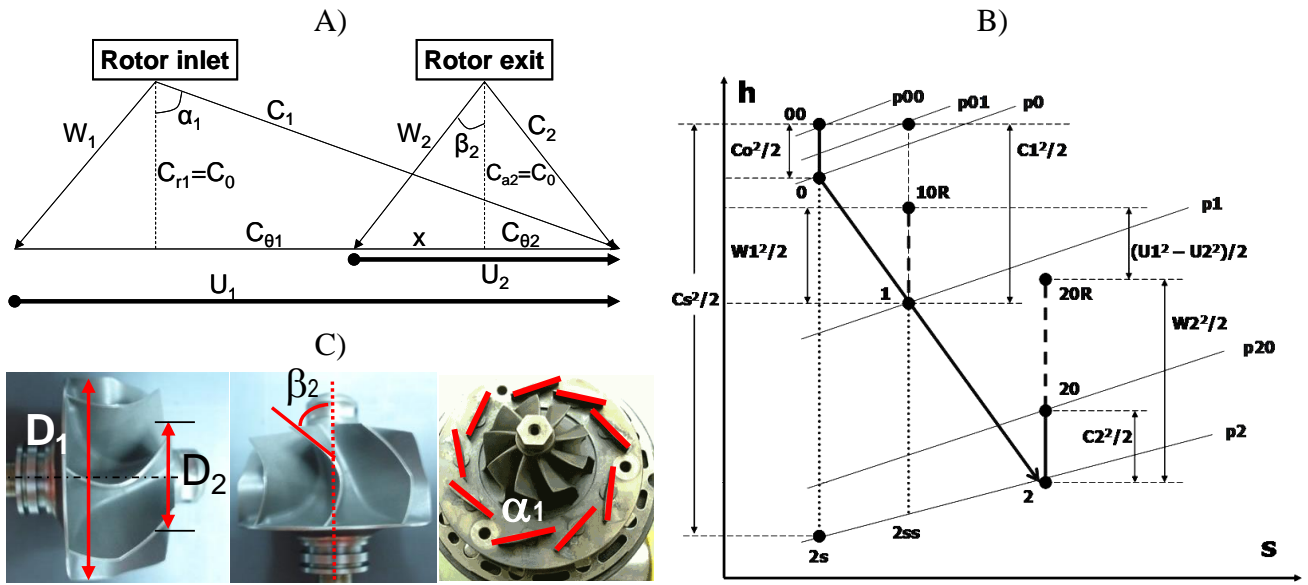


Figure 10. A) Velocity triangles for constant meridional component velocity in a radial turbine. B) Enthalpy versus entropy diagram for the turbine stage. C) Definition of dimensions and metal angles in the turbine rotor.

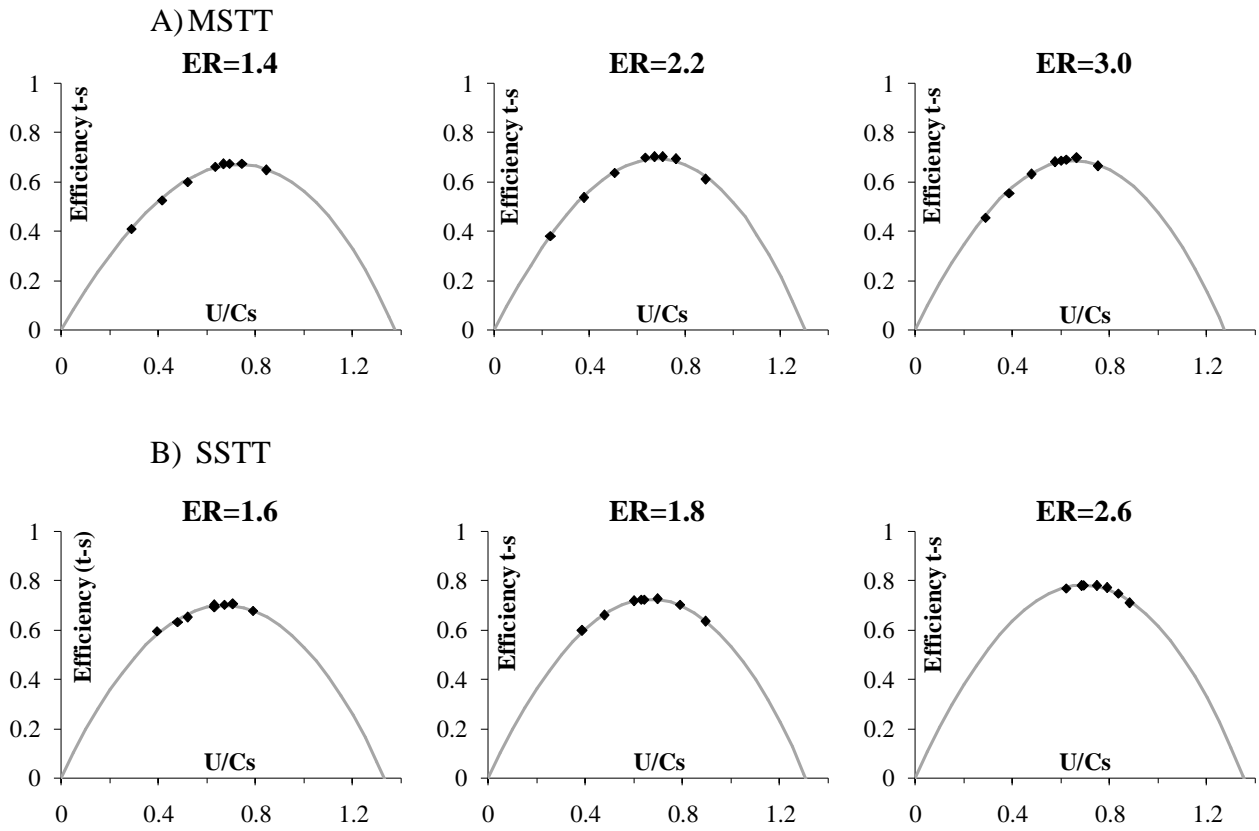


Figure 11: Isentropic efficiency fit for vaneless stator turbines; data measured at constant expansion ratio. A) MSTT. B) SSTT. Rhombus: Experimental data. Continuous line: Equation (23) predicted efficiency.

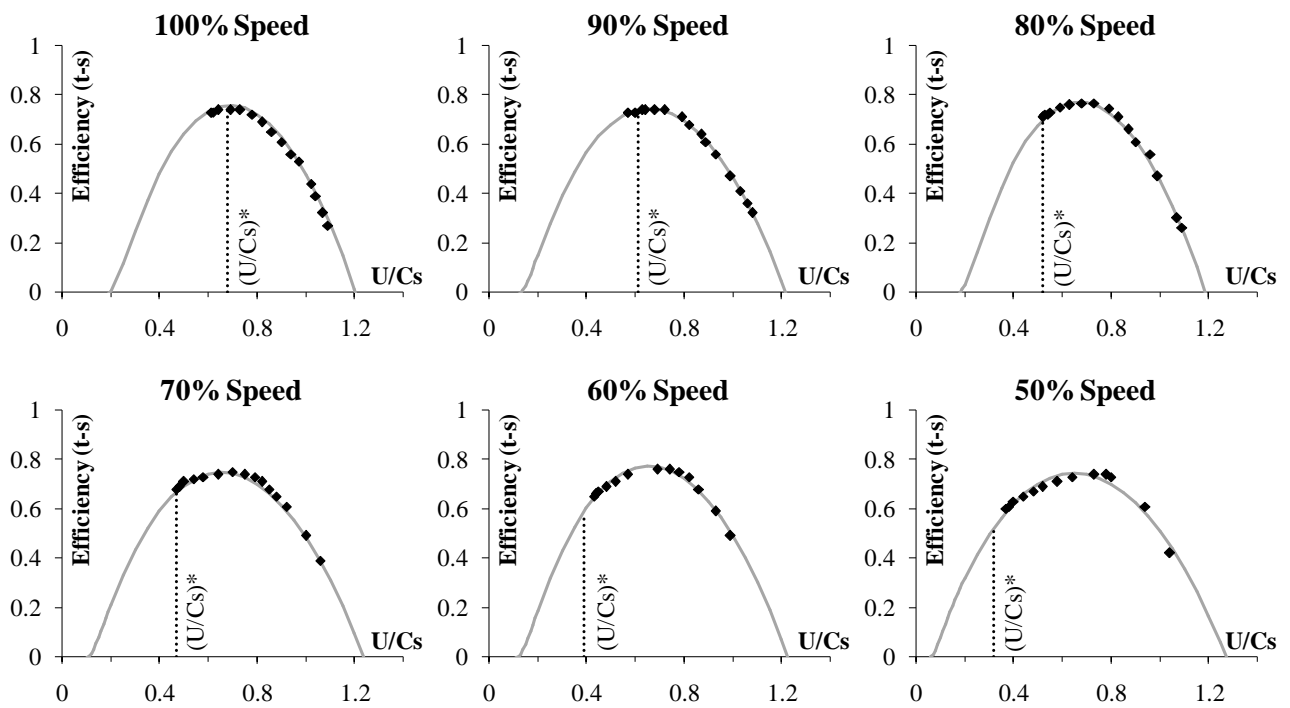
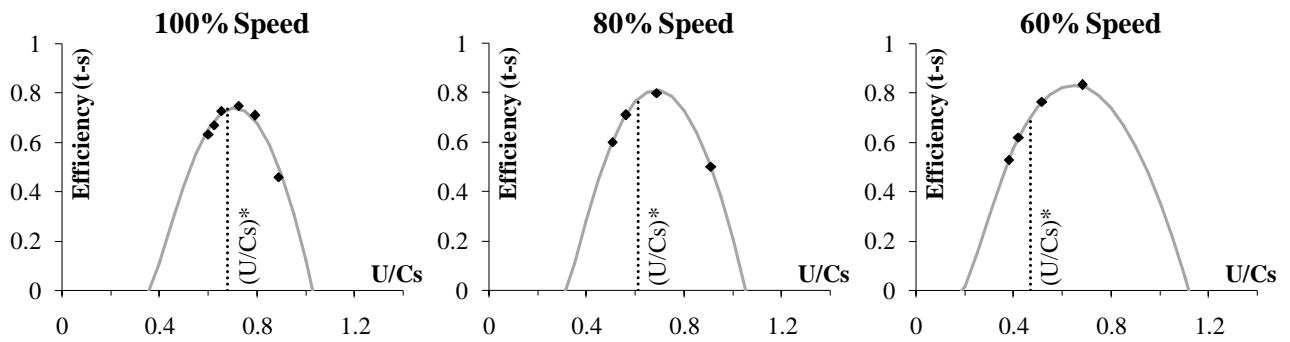


Figure 12: Isentropic efficiency fit for the vaneless stator LSTT. Experimental data measured at constant corrected speed [21]. Rhombus: Experimental data. Continuous line: Equation (27) predicted efficiency.

A) CVT [22]



B) VGT

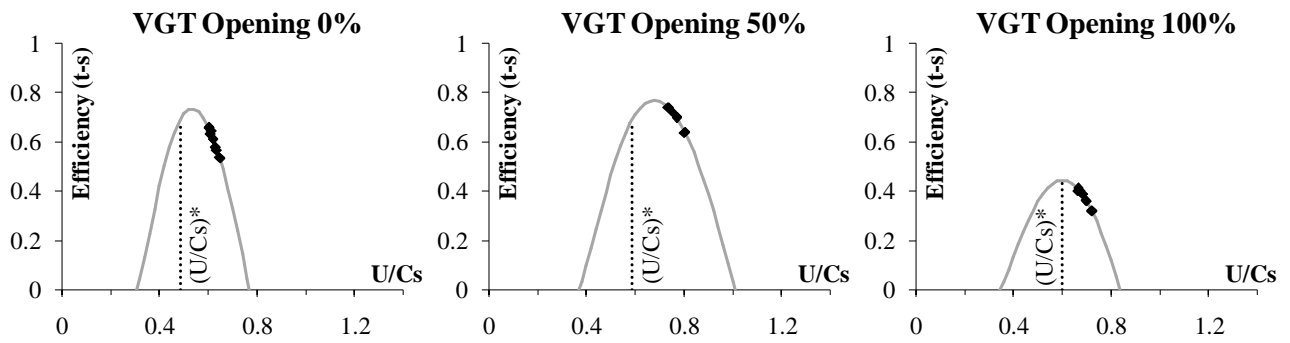


Figure 13: Isentropic efficiency fit for vaned stator turbines; data measured at constant turbocharger speed. A) CVT [22]. B) VGT. Rhombus: Experimental data. Continuous line: Equation (23) predicted efficiency.

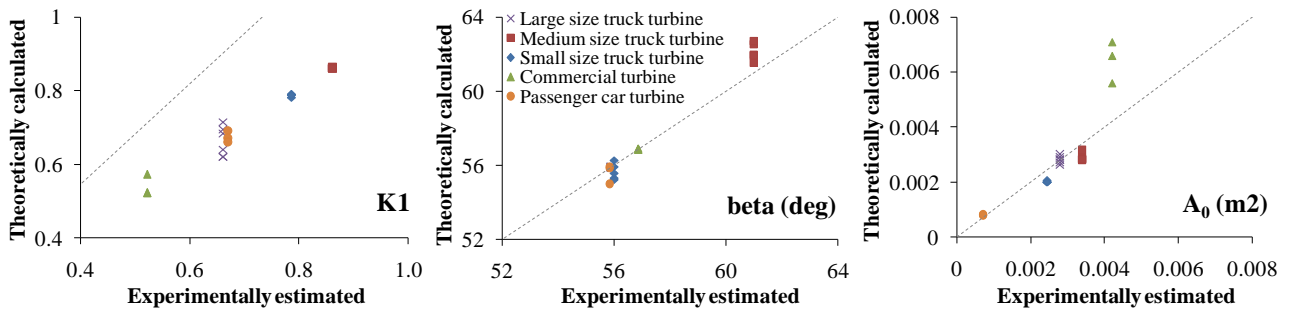


Figure 14:  $K1$  coefficient,  $\beta_2$  angle and  $A_0$  for five turbines from the studied set.

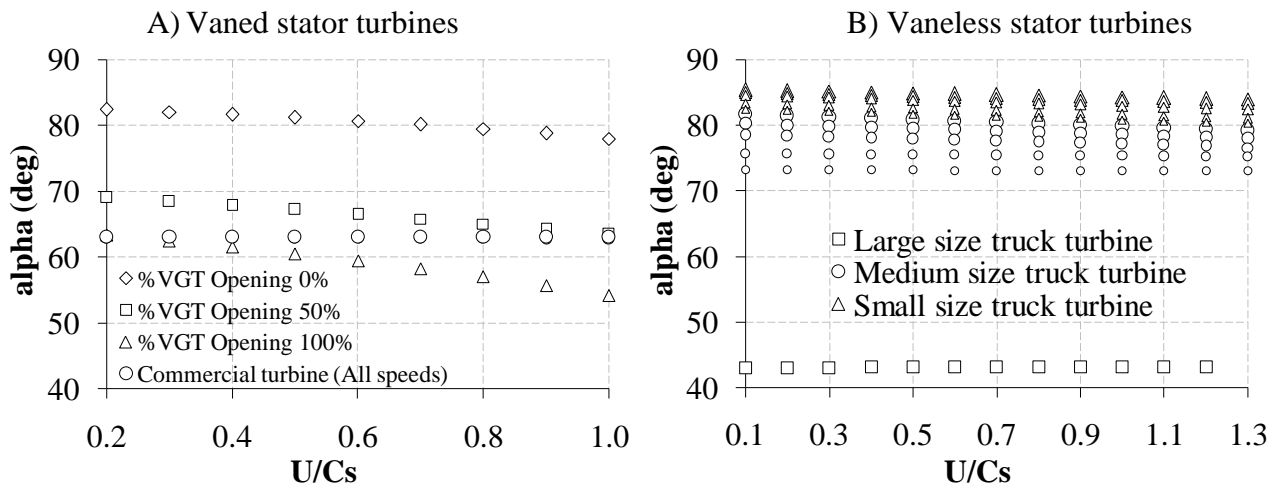


Figure 15: Variation of  $\alpha_1$  versus blade to speed ratio. A) Example turbines with vaned stator. B) Example turbines with vaneless stator. In B) chart size reduction in triangles and circles indicates expansion ratio reduction for a given turbine.